nature neuroscience

# Thalamic synchrony and the adaptive gating of information flow to cortex

Qi Wang[1,2], Roxanna M Webber[3] & Garrett B Stanley[1]

**Although it has long been posited that sensory adaptation serves to enhance information flow in sensory pathways, the neural basis remains elusive. Simultaneous single-unit recordings in the thalamus and cortex in anesthetized rats showed that adaptation differentially influenced thalamus and cortex in a manner that fundamentally changed the nature of information conveyed about vibrissa motion. Using an ideal observer of cortical activity, we found that performance in detecting vibrissal deflections degraded with adaptation while performance in discriminating among vibrissal deflections of different velocities was enhanced, a trend not observed in thalamus. Analysis of simultaneously recorded thalamic neurons did reveal, however, an analogous adaptive change in thalamic synchrony that mirrored the cortical response. An integrate-and-fire model using experimentally measured thalamic input reproduced the observed transformations. The results here suggest a shift in coding strategy with adaptation that directly controls information relayed to cortex, which could have implications for encoding velocity signatures of textures.**



Adaptation is a ubiquitous property across a large variety of areas within different sensory pathways of the brain[1–6]. Although typically associated with an attenuation of neural activity resulting from several different biophysical mechanisms, adaptation is thought to enhance the flow of information transmission in sensory pathways in complex environments[7]. Computational studies have quantitatively demonstrated that adaptation maintains information rates in the face of changes in the statistics of the sensory input[5,6]. Consistent with these notions, psychophysical studies have shown that adaptation to a periodic tactile input enhances human performance in both amplitude and frequency discrimination[8–10]. The precise link between the changes in coding properties and the feature representation in the various stages of processing that underlies perception, however, remains poorly understood.

Owing to the well studied feed-forward anatomy, the thalamus is classically described as a relay station between the sensory periphery and the cortex. However, the complex dynamic interaction between the thalamic and cortical structures is perhaps the key element in establishing representations that ultimately result in perception of our sensory environment. It has been asserted that thalamic gating can shift coding properties of the pathway between detecting salient features of the sensory environment and transmitting details of the sensory environment[11,12]. By taking the perspective of an ideal observer of thalamic activity and decoding elements of the sensory input, we have previously shown that high-frequency thalamic bursting is selective for detecting salient features in the natural sensory input[13]. Short interspike intervals of single thalamocortical neurons[14] and synchronous activity across multiple thalamic neurons projecting to a common cortical target[15,16] are significantly more likely to evoke spiking in the downstream cortical neuron, consistent with the notion of a "window of opportunity" for integration for the cortical cell[17]. It has recently been shown that adaptation strongly shapes thalamic synchrony[18] and dictates the window of integration of the recipient cortical target[19]. How this shapes not only how much, but what kind of information is conveyed to the cortex, is unknown.

Here, through simultaneous single-unit recordings in the ventral posteromedial (VPm) nucleus of the thalamus and cortical layer 4 in the rat vibrissal pathway during controlled vibrissa movements in the anesthetized rat, we show that sensory adaptation differentially influences thalamic and cortical activity in a manner that fundamentally changes the nature of the information conveyed about the sensory input. Specifically, from the perspective of an ideal observer of spiking activity, the cortical neurons show a degraded performance in detecting vibrissal deflections with adaptation, while showing an enhancement in discriminating between deflections of different velocities. Paired recordings in topographically aligned neurons in the VPm thalamus revealed no such trend in the projecting input to cortex, also reflected in putative monosynaptic pairings. Analysis of simultaneously recorded thalamic neurons did unveil, however, an analogous adaptive change in thalamic synchrony that mirrors the observations of cortical response magnitude. A simple leaky integrate-and-fire network model using experimentally measured thalamic input reproduces the observed transformations from thalamus to cortex. Taken together, the results here suggest an adaptive shift in the coding strategy that has direct functional consequences regarding the nature of information relayed to cortex.

## RESULTS

Single-unit, extracellular recordings were made of putative excitatory neurons (regular spiking units (RSUs); see **Fig. 1a**, left, for a typical RSU waveform) in layer 4 of the vibrissal region of the primary

[1]Coulter Department of Biomedical Engineering, Georgia Institute of Technology & Emory University, Atlanta, Georgia, USA. [2]School of Engineering & Applied Sciences, Harvard University, Cambridge, Massachusetts, USA. [3]Department of Neurobiology, Harvard Medical School, Boston, Massachusetts, USA. Correspondence should be addressed to G.B.S. (garrett.stanley@bme.gatech.edu).

Received 5 August; accepted 21 September; published online 21 November 2010; doi:10.1038/nn.2670

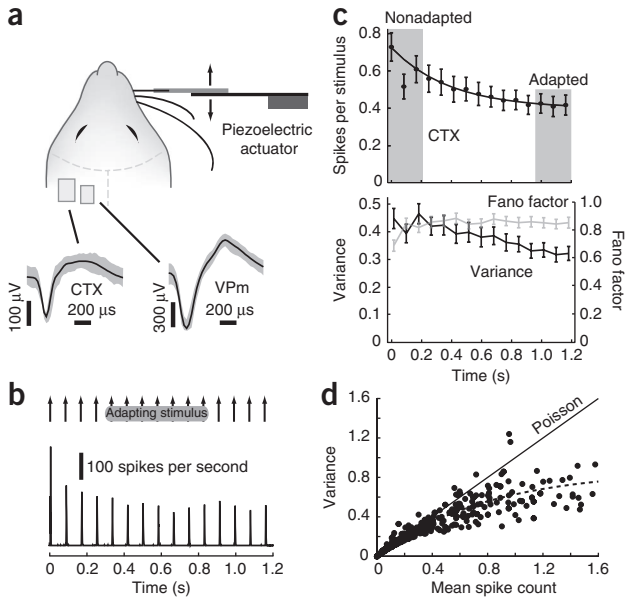


**Figure 1** Statistical properties of cortical response adapt to vibrissa deflections. (**a**) Example waveforms from recordings in the thalamic VPm (right) and cortical layer 4 (CTX, left). Single-unit extracellular recordings were made during movement of the identified primary vibrissa in the rostral–caudal plane using a computer-controlled piezoelectric bending actuator. Gray bands denote ± 1 s.d. (**b**) Adaptation in the PSTH (2-ms bin size) for a typical cortical regular spiking unit (RSU) in response to a 12-Hz sequence of punctate vibrissa deflections (15 cycles, 800 deg $s^{-1}$; see Online Methods). (**c**) Top: mean spike count (in 30-ms bin following each deflection) across the sample ($n = 30$ cortical RSUs). Curve is an exponential fit using least squares, excluding the outlier in response to the second pulse. Bottom: corresponding spike count variance (left axis) and Fano factor (variance/mean, right axis), across the cortical sample. (**d**) Cortical firing statistics. Each data point represents the response in a 30-ms window following the probe stimulus. Dashed line shows exponential fit of relationship, as compared to the Poisson case for which the variance equals the mean (solid line). In general, response was sub-Poisson, with trial-to-trial spike count variance less than the mean for high spike counts. Error bars are ± 1 s.e.m.

somatosensory cortex, in response to controlled deflection of the corresponding primary vibrissa (see **Fig. 1a** and **Supplementary Fig. 1** for all cortical units in the main data set of the study). Cortical neurons adapted strongly to persistent, ongoing sensory stimuli, as shown by the peri-stimulus time histogram (PSTH) of evoked activity from a typical neuron in **Figure 1b** in response to a 12-Hz periodic vibrissa deflection pattern.

In response to these transient vibrissa motions, cortical neurons showed an exponential reduction in spike count from the stimulus onset (nonadapted) to steady-state (adapted) (**Fig. 1c**, top panel; sample, $n = 30$). The reduction in spike count from the nonadapted to adapted states was quantified by the adaptation ratio (ratio of adapted spike count to nonadapted, see Online Methods), which was 67% here, consistent with other studies using similar experimental methodologies[3,4]. The reduction in spike count with adaptation was accompanied by a corresponding reduction in trial-to-trial spike count variance (**Fig. 1c**, bottom). The relationship between the mean and variance was nonlinear, following a sublinear exponential rise to an apparent saturation (**Fig. 1d** and **Supplementary Fig. 2**).

## Detection and the ideal observer

Taking the computational perspective of an ideal observer of the cortical response, we can ask to what extent we can detect the presence of a vibrissa deflection, and how this is affected by adaptation. The observer algorithm was asked to indicate whether or not a vibrissa deflection was presented after a cue marking the stimulus onset (**Fig. 2a**; see Online Methods for observer algorithm). This can be envisioned as discrimination between signal and noise, in the classical signal detection theory framework.

The observer was challenged with this question before (nonadapted) and after (adapted) the pathway was presented with an adapting periodic vibrissa deflection. The ideal observer made the decision based on the summed activity across multiple trials, assumed to represent the aggregate population spike count[20,21] (see Online Methods). An example of the corresponding distributions in the presence (signal) and absence (noise) of a vibrissa deflection for a typical cortical RSU is shown in **Figure 2b**. Plotted are the parametric fits of the

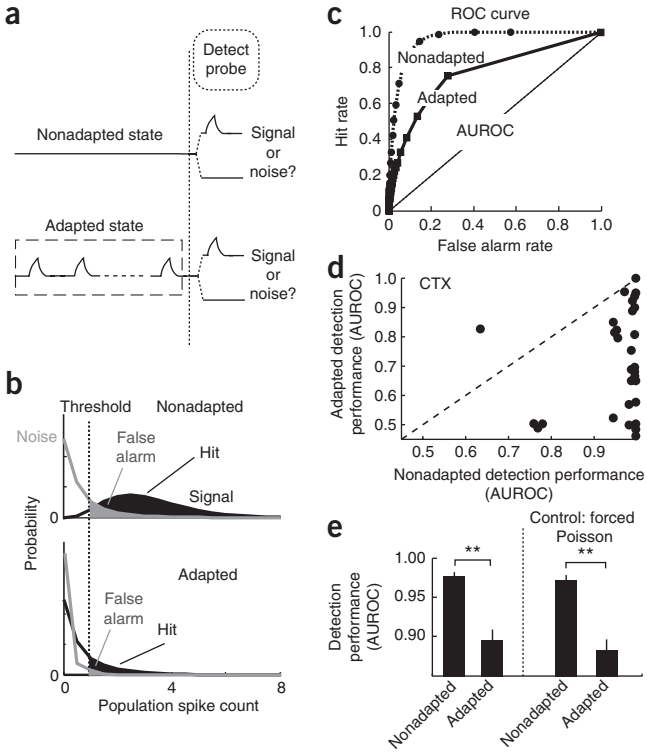


**Figure 2** Adaptation degrades stimulus detection for ideal observer of cortical activity. (**a**) Observer attributes response to 'signal' or 'noise', in the presence (adapted) and absence (nonadapted) of a preceding adapting stimulus (15 cycles of a 12-Hz sequence of a punctate deflection at 800 deg $s^{-1}$). (**b**) Variations in spike count from trial to trial establish distributions for the signal (black) and the noise (gray) (parametric fits of raw data; **Supplementary Note 1**), in both the nonadapted (top) and adapted (bottom) states. Above a threshold, the observed spike count was attributed to signal; below, to noise. The mean spontaneous firing rate decreased from 0.68 ± 0.093 Hz in the nonadapted state to 0.42 ± 0.064 Hz in the adapted state (mean ± s.e.m., $P < 0.01$, Wilcoxon signed-rank test). (**c**) The area under the ROC curve was used as a metric for overall performance (AUROC). Diagonal represents chance performance, where probability of false alarm and hit are equal and AUROC is 0.5. (**d**) Performance (AUROC) in the detection task in the nonadapted versus adapted states ($n = 30$ cortical (CTX) RSUs) for the lowest velocity used for the probe. The dashed line is the unity line. (**e**) Detection performance for the entire range of probe velocities. Control is the resultant performance when the spike count variance was forced to equal that of the experimentally observed mean spike count in the nonadapted and adapted states (**Supplementary Note 2**). Performance was significantly better in the nonadapted state than in the adapted (** $P < 10^{-19}$, ** $P < 10^{-20}$ for control, Wilcoxon signed-rank test). Error bars are ± 1 s.e.m.

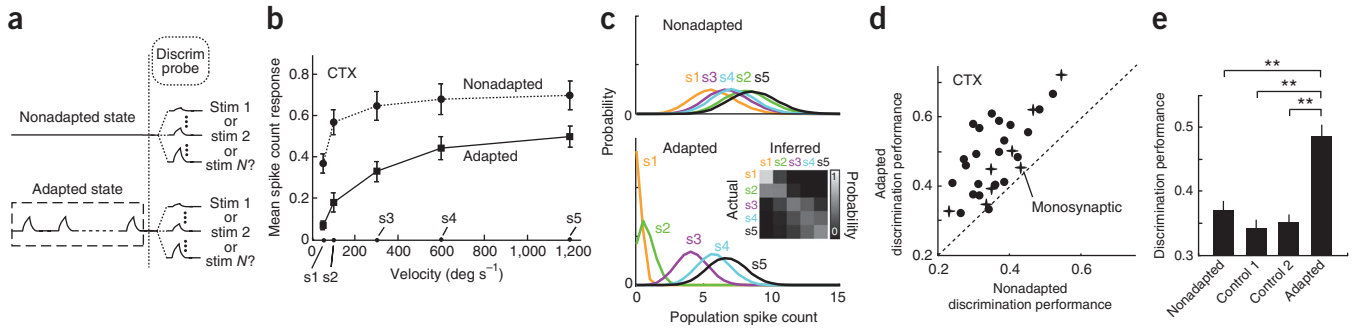


**Figure 3** Adaptation enhances cortical discriminability. (**a**) In the discrimination (discrim) task, observer attributes spike count to one of several possible stimuli (stim), in the presence (adapted) and absence (nonadapted) of a preceding adapting stimulus. (**b**) Mean sensitivity of the cortical (CTX) response to the deflection velocity in the nonadapted (dotted) and adapted (solid) states ($n = 30$ cortical RSUs). The velocities to be discriminated between (s1–s5) are noted on the horizontal axis. (**c**) Population spike count distributions for a typical cortical neuron for the velocities (s1–s5) in the nonadapted (top) and adapted (bottom) states. Adaptation attenuated the response but also separated the distributions. Shown in the inset is the performance matrix (see Online Methods). (**d**) The overall discriminability performance, quantified as the fraction of correct identifications. The crosses represent cortical neurons that were identified as monosynaptic recipients of VPm inputs (**Fig. 5**). (**e**) Discrimination performance was significantly better in the adapted state than in the nonadapted state ($n = 30$ cortical RSUs, $^{**}P < 3 \times 10^{-4}$ for non-adapted, $^{**}P < 1 \times 10^{-4}$ for control 1 and control 2, Wilcoxon signed-rank test). Control 1 is the case in which the mean spike count in response to each velocity in the nonadapted state was attenuated by deleting 33% of the spikes to match the observed overall spike count reduction with adaptation. Control 2 is the case in which the mean and variance in the nonadapted state were scaled down 33% to match the spike count reduction caused by the adaptation (**Supplementary Note 2**). In both control cases, there was no difference in performance from the nonadapted state (control 1, $P = 0.12$; control 2, $P = 0.25$; Wilcoxon signed-rank test). Error bars are ± 1 s.e.m.



experimentally measured distributions (**Supplementary Fig. 3a** and **Supplementary Note 1**). The signal in this case was a weak, punctate vibrissa deflection of 50 deg $s^{-1}$. In the spike count distributions for the nonadapted case (**Fig. 2b**, top), the mean population spike count was of course larger for the signal than for the noise, but both showed some degree of variability, leading to overlap in the distributions. Classical signal detection involves the selection of a threshold, above which the response is classified as signal, and below which as noise. The area under the response distribution to the right of the threshold when a signal was actually present (black) is the probability of a correct detection ('hit'), whereas the corresponding area under the response distribution in the absence of signal (gray) is the probability of an incorrect attribution of the observed response to signal when it was actually noise ('false alarm'). Given the effect of adaptation on the spike count, we expected that the mean population spike count for the vibrissa deflection would decrease (**Fig. 2b**, bottom). In addition to the mean population spike count, adaptation decreased the variance and significantly altered the noise distribution (spontaneous activity). Together, these changes affected the degree of overlap between the signal and noise distributions.

The performance of the observer was quantified using a receiver operating characteristic (ROC) analysis[20,21], which captures the probability of false alarms versus correct detections as a function of the choice of thresholds (**Fig. 2c**). Because the performance varies with the choice of threshold, the total area under the ROC curve (AUROC) was used as a single metric of overall performance, where a value of 1 indicates a false alarm rate of 0 and a hit rate of 1, and a value of 0.5 indicates chance. For this particular cortical neuron, for a given angular velocity, the AUROC was significantly larger for the nonadapted state than for the adapted. For the larger sample ($n = 30$) (**Fig. 2d**), there was a significant degradation in detection performance with adaptation (**Fig. 2e**, left; $P < 10^{-19}$). A control analysis showed that this effect was not due to the sublinear decrease in variance with adaptation (**Fig. 2e**, right, and **Supplementary Note 2**). Note that the detection performance (**Fig. 2e**) was evaluated for a range of probe velocities, showing an overall higher level of performance as compared to the scatter plot for the low velocity probe (**Fig. 2d**).

## Discrimination and the ideal observer

Again taking the perspective of an ideal observer of the cortical response, we can ask to what extent we can discriminate between different sensory inputs, and how this is affected by adaptation. The observer was asked to discriminate between vibrissa deflections of different velocities (**Fig. 3a**). The observer was challenged with this question in the presence (adapted) or absence (nonadapted) of previously adapting periodic vibrissa deflections (**Fig. 3b**). It is clear that the adaptation attenuated the response magnitude for all stimuli (velocities). However, the difficulty of the task of the observer depended upon the overlap in distributions of the responses to each of the velocities. In the response distributions of an example cortical neuron to five different angular velocities of vibrissa deflection (50, 100, 300, 600 and 1,200 deg $s^{-1}$; stimuli s1, s2, s3, s4, s5, respectively; **Fig. 3c**), the spike counts were relatively high in the nonadapted case (top), but the distributions were highly overlapped, and even unordered (parametric fits of experimentally observed distributions, **Supplementary Fig. 3b**). In contrast, in the adapted case (bottom), the spike counts were attenuated, but the distributions became more separated and ordered. Note that the stimulus design held the duration of the punctate stimulus fixed, and thus the peak amplitude of the deflection co-varied with the velocity (see Online Methods).

To quantify the effects of this transformation on the performance of the ideal observer in discriminating between different deflection velocities, we used a Bayesian decoder to estimate the most likely velocity presented from the observed cortical response, given a uniform prior (that is, each velocity was presented with equal probability) (**Supplementary Note 1** and **Supplementary Fig. 4**). The performance matrix (**Fig. 3c**, inset) displays the probability of inferring a particular velocity for each of the actual velocities presented. The overall metric of performance reflects the fraction of correctly identified stimuli (chance would be 20%, or 0.2). In contrast to the detection task, the observer was significantly better at discriminating between different velocities in the adapted state than in the nonadapted state (**Fig. 3d**,**e**; $P < 3 \times 10^{-4}$). Control analysis showed that the change in performance with adaptation observed in the data was not a trivial consequence of the attenuated response in the adapted state, but instead relied on

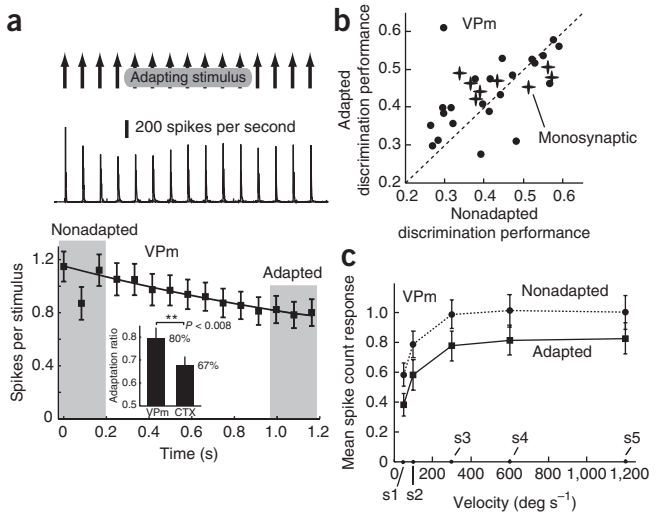


**Figure 4** Cortical performance does not trivially mirror activity of thalamic projections. (**a**) For each cortical recording, a VPm neuron in the homologous barreloid was recorded simultaneously. The VPm neurons adapted to the persistent, ongoing periodic vibrissa deflection but showed less attenuation in the response (PSTH for a typical example: 1-ms bin, mean spike count across the larger sample, $n = 32$ VPm units). Curve is an exponential fit using least squares, excluding the outlier in response to the second pulse. The inset shows the adaptation ratio for the cortical (CTX) RSUs (67%) and VPm (80%) neurons. (**b**) Discrimination performance in the nonadapted versus adapted states for the recorded VPm units ($n = 32$). Highlighted with crosses are those that were identified as monosynaptically connected to the RSUs highlighted in **Figure 3d**. Adaptation did not affect the discrimination performance for an ideal observer of VPm spike count ($P = 0.19$, $n = 32$, Wilcoxon signed-rank test). (**c**) In contrast to the sensitivity curve in cortex, the sensitivity curve in VPm retained its shape after adaptation, resulting in little or no change in overall sensitivity and thus no change in performance. Error bars are ± 1 s.e.m.

the nonuniform changes in the separation between the distributions with adaptation (**Fig. 3d**,**e** and **Supplementary Note 2**).

In addition to the obvious adaptation effects on the spike count, the average overall shape of the sensitivity curve changed with adaptation, from a step function form to one that showed a more gradual change in response with increased stimulus strength (**Fig. 3b**). The adaptation thus provided sensitivity over the range of angular velocities tested here. Taken together, the results of the detection and discrimination performance analysis show that adapting cortical neurons switched from a state in which detection was favored to a state in which discrimination was favored. Notably, in an additional set of experiments, we found that adaptation enhanced discriminability between deflections of the vibrissa in different angular directions, pointing to a general phenomenon (**Supplementary Note 3** and **Supplementary Fig. 5**).

## Thalamic input

Given the observations regarding the switch in performance with adaptation in the cortical response, it is important to ask how these properties arise. It may simply be the case that the cortex is trivially inheriting these properties from the projecting thalamic input. Neurons in the ventral posteromedial nucleus (VPm) of the thalamus do also adapt in response to persistent, ongoing sensory input in a manner similar to that in cortex, albeit to a lesser degree. Each of the cortical neurons in **Figures 1**–**3** was recorded while simultaneously recording from a topographically aligned VPm neuron (that is, in the homologous barreloid; see **Fig. 1a**, inset, for typical VPm spike waveform, and **Supplementary Fig. 6** for all thalamic units in the main data set). In a PSTH for a typical VPm neuron and the mean decay in VPm spike count in response to the same 12-Hz repetitive stimulus (**Fig. 4a**; for two recording sessions, two VPm units were recorded on separate electrodes of the multi-electrode positioned in thalamus), the VPm PSTH showed a fairly rapid decrease in amplitude, whereas the spike count decay was much more gradual, consistent with previous observations[22].

Although the adaptation response was qualitatively similar to that in the cortical neurons, VPm neurons showed weaker adaptation and a correspondingly larger adaptation ratio of 80% (as compared to 67% for the cortical RSUs in **Fig. 1c**; $P < 0.008$, Mann-Whitney *U*-test) (**Fig. 4a**, inset). An ideal observer of the VPm spike count was then challenged with the same detection and discrimination tasks as above. Although the VPm detection performance did degrade with adaptation owing to the lower spike count ($P < 0.003$, $n = 32$, Wilcoxon signed-rank test; **Supplementary Fig. 7**), the adaptation produced no change in discrimination performance, in contrast to observations in cortex (**Fig. 4b**; $P = 0.19$, $n = 32$, Wilcoxon signed-rank test). In contrast to their cortical counterparts, the velocity sensitivity curves for the VPm neurons showed only an overall scaling of the magnitude of the spike count with adaptation (**Fig. 4c**), as opposed to a fundamental change in shape of the sensitivity in cortex that gave rise to the change in performance (**Supplementary Fig. 8**).

To rule out the possibility that the observed discrepancy between changes in thalamic and cortical discrimination performance with adaptation was due to experimental methods or selection bias in the neural recordings, we analyzed the simultaneously recorded VPm and cortical activity in a pairwise manner. First, a small subset of the thalamocortical pairs was conservatively identified as having monosynaptic connectivity (that is, the recorded VPm neuron served as direct input to the layer 4 cortical neuron; crosses in **Figs. 3d** and **4b**). This assessment was performed using spike cross-correlation analysis in the presence of a very weak vibrissa stimulation (Online Methods)[23,24].

In an example of the shuffle-corrected spike cross-correlogram for a typical pair (**Fig. 5a**), the emergent peak at approximately 2 ms was consistent with monosynaptic connectivity across the thalamocortical structures[14,23]. The inset shows the average correlograms across the subset of pairs we identified as monosynaptically connected ($n = 8$ pairs). For this subset of pairs, the discrimination performance was significantly better in the adapted state than in the nonadapted state for the cortical cell (**Fig. 5b**, left) ($P < 0.007$, Wilcoxon signed-rank test), whereas the VPm cell showed no difference (**Fig. 5b**, right) ($P = 0.84$, Wilcoxon signed-rank test). The primary result here thus held for the conservatively identified connected pairs. Further, it is likely that many of the other recorded pairs were also connected pairs but did not meet the stringent requirements imposed here[24]. The pairwise percent change in discrimination performance from the nonadapted to adapted state for each of the simultaneously recorded VPm and cortical pairs (**Fig. 5c**) showed little or no trend in performance for the VPm while showing an enhanced performance for the cortex. The increase in cortical discrimination performance with adaptation was significantly greater than that in VPm (comparison of performance ratios, $P < 0.001$, Student's *t*-test; see Online Methods).

## Thalamic synchrony affects cortical performance

The above results suggest that the cortical shift in performance was not trivially inherited from the projecting thalamic input. However, this does not completely preclude an explanation of the cortical response properties from the thalamic population input. Timing across the thalamic population is a critical component in establishing

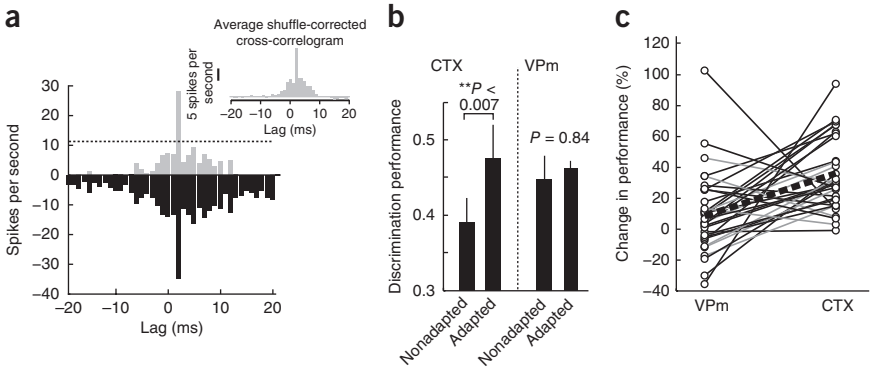


**Figure 5** Shift in discrimination performance is maintained in monosynaptically connected thalamocortical pairs. (**a**) An example of the raw (reflected about the horizontal axis) and shuffle-corrected correlograms for a particular VPm–cortex (CTX) pair, along with the corresponding >99% confidence interval (3 s.d.) on an uncorrelated process (dotted line). The inset shows the average shuffle-corrected correlogram for the eight pairs. VPm–CTX pairs were identified as monosynaptically connected on the basis of the presence of a statistically significant, short-latency peak in the spike train cross-correlation function for weak 4-Hz sinusoidal vibrissa stimulation. (**b**) The results for the larger sample (**Figs. 3** and **4**) held for the smaller, monosynaptically connected sample (CTX, $^{**}P < 0.007$; VPm, $P = 0.84$; Wilcoxon signed-rank test). (**c**) Percent change in discrimination performance from nonadapted to adapted states for each VPm–CTX pair. Gray lines denote pairs identified as likely to be monosynaptically connected. Thick dashed line shows the mean performance change. Error bars are ± 1 s.e.m.

feature selectivity in cortex. In a separate set of experiments, we used a multi-electrode to record simultaneously from VPm pairs within the same barreloid in response to the adapting stimulus (see Online Methods). As the VPm adapted in response magnitude (spike count), we observed a desynchronization of the thalamic response. The mean synchrony decreased with the adapting stimulus (**Fig. 6a**), where synchrony was defined as the central area under the spike cross-correlogram (±7.5 ms, see Online Methods and **Supplementary Note 4**); that is, the probability, given a spike of one VPm neuron, of observing a spike from the other VPm neuron within ±7.5 ms.

The synchrony across VPm neurons was also modulated by the vibrissa deflection velocity (**Fig. 6a**,**b**). The different velocities (s1–s5) elicited greater variation in the synchrony across the pairs in the adapted than in the nonadapted state (**Fig. 6a**). The adaptation acted to attenuate thalamic synchrony, while simultaneously increasing the sensitivity of thalamic synchrony to velocity (**Fig. 6b**). This can be seen in the shape of the synchrony curve in the adapted state, reminiscent of the cortical spike count curve shown in **Figure 3b**. Although the presence and importance of noise correlations has recently been described for this pathway[18], the effects here were largely stimulus driven, as the noise correlations were comparatively small and relatively insensitive to deflection velocity (linear regression, $P = 0.32$ for nonadapted and $P = 0.35$ for adapted; see **Supplementary Fig. 9**).

The importance of the above observation becomes clear in considering the role of timing across thalamic neurons in determining the response of the downstream layer 4 cortical target, given the relative timing of firing across a small population of VPm neurons and the effects of the stimulus strength on the degree of synchronization of these responses (**Fig. 7a**). Previous studies of the thalamocortical circuit have demonstrated that adaptation modulates the integration window of the thalamic influence on the recipient layer 4 neurons[19]. Specifically, adaptation delays the arrival of feedforward inhibitory inputs, increasing the window of opportunity for feedforward excitatory thalamic input. The integration window of the recipient cortical cell is 12 ± 2 ms in the nonadapted case versus, 22 ± 2 ms in the adapted[19]. In the nonadapted case, the changes in the synchronization with stimulus strength are small relative to the integration window, thus leading to a relative insensitivity of the cortical response to stimulus strength (velocity). In contrast, in the adapted case, although the integration window is wider as compared to the nonadapted state, the overall synchrony is less, and more importantly, the changes in synchrony with changes in deflection velocity are pronounced. This leads to spiking of some of the VPm cells outside the window of integration and thus a less efficacious input to drive the recipient cortical target.

### Detection, discrimination and window of opportunity

The above qualitative assertion can be demonstrated quantitatively through the use of a simple leaky integrate-and-fire model of the cortical response to incoming VPm inputs (**Fig. 7b**). The degree of synchrony was nearly identical across simultaneously recorded VPm pairs when the trials were randomly shuffled relative to each other

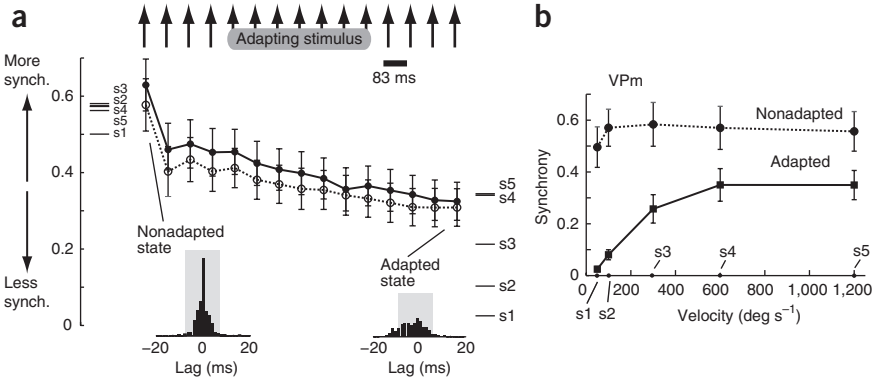


**Figure 6** Thalamic population synchrony is modulated by adaptation. (**a**) Synchrony (synch.) was measured as the central area under the cross-correlogram (± 7.5 ms; see **Supplementary Note 4** and **Supplementary Fig. 10**). Shown also are the measures of synchrony for the five velocities to be discriminated among, in the nonadapted (left) and adapted (right) states. The inset shows the spike cross-correlograms in the nonadapted and adapted states. For VPm pairs recorded simultaneously, the adaptation served to reduce the timing precision across neurons, or desynchronize their firing activity ($n = 19$ pairs). When the trials were shuffled (dotted line, open symbols), the resulting synchrony in response to the velocity was unchanged. (**b**) Synchronous firing across VPm pairs ($n = 19$ pairs) as a function of deflection velocity, in both the nonadapted (dotted, circle) and adapted states (solid, square).

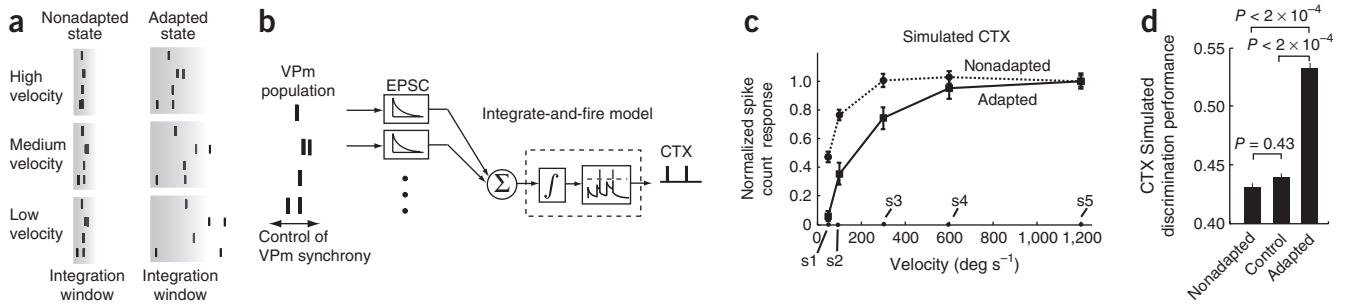


**Figure 7** Thalamocortical network model predictions. (**a**) Thalamic spiking that falls within the cortical integration window is relayed to cortex. In the nonadapted state (left), velocity effects on synchrony of VPm activity are small, and signals are strongly relayed to cortex. In the adapted state (right), the integration window widens, and the velocity strongly modulates the VPm synchrony. At lower velocities, VPm spiking falls outside the integration window and does not relay to cortex. (**b**) The spiking activity from a population of VPm neurons was used as the input to an integrate-and-fire model of the cortical response. Firing of a VPm input generates an excitatory postsynaptic current (EPSC), the sum of which is integrated in the model to affect the cortical membrane potential. Upon crossing a threshold, the model cortical cell (CTX) fires a spike, then resets. (**c**) Velocity sensitivity curves for the simulated cortical response in the nonadapted (dashed) and adapted (solid) states, both normalized to their peak spike count. (**d**) The change in thalamic synchrony with adaptation served to increase performance in discriminating between different velocities, as judged by cortical spike count response ($P < 2 \times 10^{-4}$ versus non-adapted and control, Wilcoxon signed-rank test). The control shows the case where the adaptation produced changes in the VPm spike count, as observed, but the degree of synchrony was maintained in the nonadapted state, resulting in a loss in performance in the adapted state. Control was not different from non-adapted ($P = 0.43$, Wilcoxon signed-rank test). Error bars are ± 1 s.e.m.



(**Fig. 6a**), suggesting that the VPm pairs had very weak noise correlations compared to the stimulus-driven correlations. Although the weak pairwise correlations might have a function in the behavior of the network at a larger scale[25], we focused on the stimulus-driven correlations (see Discussion). In the model, a random selection of trials across all recorded VPm neurons was used as a surrogate for the population VPm response on a single trial. The thalamic population input corresponding to a particular deflection velocity (s1–s5) was generated from ten trials of experimentally recorded VPm activity corresponding to that particular velocity, randomly drawn across all recorded VPm cells and trials. The VPm population firing produced simulated excitatory postsynaptic currents (EPSCs) that were spatially summed, capturing the total synaptic drive of the cortical RSU. This input was integrated, yielding an instantaneous measure of the membrane potential of the model cortical cell. Action potentials were generated when the potential crossed a threshold, at which point the integrator was reset (see Online Methods for a description of the model membrane properties). The 'window of opportunity' was assumed to follow that described previously, where adaptation delays the arrival of feedforward inhibitory inputs, increasing the window of opportunity for feedforward excitatory thalamic input to generate downstream suprathreshold activity[19]. In the nonadapted state, the recorded VPm activity is sufficiently synchronous as not to affect the cortical response. The resulting cortical response in the nonadapted state thus reflected primarily the fraction of VPm units firing. Because the VPm spike count was relatively insensitive to vibrissa deflection velocity in the nonadapted state, the cortical spike count was also relatively insensitive to velocity. In contrast, however, in the adapted state, the VPm input was less synchronous, and the degree of synchrony was more sensitive to the velocity than in the nonadapted state (**Fig. 6b**). Weaker stimuli resulted in loss of synchrony. As a result, despite the lack of VPm spike count sensitivity to velocity, the model cortical spike count was sensitive to velocity (**Fig. 7c**). The model prediction was very similar to the experimental findings in **Figure 3b** (**Supplementary Fig. 8b**,**d**). As a result, there was an increase in discrimination performance from the nonadapted to adapted states (**Fig. 7d**; $P < 2 \times 10^{-4}$, $n = 30$ simulated neurons, Wilcoxon signed-rank test), as we observed in experimental data (**Fig. 3e**).

To confirm that the enhancement of cortical discrimination performance was due to adaptation of thalamic synchrony, and to rule out the contribution of VPm spike count in the observed phenomena, we performed a control analysis: spikes were removed from the nonadapted VPm responses according to the observed thalamic adaptation ratio of 80% (that is, 20% of the spikes were removed) to create the hypothetical adapted VPm input for the adapted state. In other words, we preserved the experimentally observed VPm spike count in the adapted state, but eliminated adaptation effects on the synchrony. This control adapted VPm sensitivity curve thus was the same as the experimentally observed curve in **Figure 4d**, but the synchrony matched the nonadapted case in **Figure 6b**. Using this to drive the model, we found that this markedly degraded the discrimination performance of the resultant cortical model output (control case in **Fig. 7d** not significantly different from the nonadapted case; $P = 0.43$, Wilcoxon signed-rank test). Thus, we conclude that the adaptation effect on thalamic synchrony was the key element in the shift in cortical coding strategy with adaptation.

## DISCUSSION

Our results provide a direct link between the long-observed phenomenon of enhanced sensory performance with adaptation and the underlying neurophysiological representation in the primary sensory cortex. Here, we show that adaptation not only serves to enhance discriminability of vibrissa deflection velocities, but also to enhance discriminability of deflection angle (**Supplementary Note 3** and **Supplementary Fig. 5**), pointing to a general phenomenon. It has long been postulated that sensory adaptation serves to enhance information flow in sensory pathways[7]. Psychophysical studies have indeed shown that adaptation to a periodic tactile input on the skin surface enhances spatial localization in a two-point discrimination task in humans[10], presumably through engaging lateral inhibitory mechanisms serving to better spatially localize the cortical activation. Further, adaptation to periodic tactile input has also been shown to enhance amplitude[9] and frequency discrimination[8] in humans. Although the perceptual effects of adaptation have been studied in some detail, the link to the underlying neurophysiology has historically been much less clear. In contrast to previous studies focusing on how adaptation influences how much information is being transmitted

by the pathway[5,6], here we show that it is also important to reframe the question: What is information being transmitted about?

Neurons in the sensory cortices adapt their mean firing rates to ongoing stimuli in many different pathways. However, in the face of dynamic sensory input there is a complex, evolving interplay between excitatory and inhibitory subpopulations of cortical neurons that affects the population activity across the thalamocortical structures in a more subtle, and computationally rich, manner[22,26]. For example, the excitatory and inhibitory inputs to cortical cells dynamically adapt in response to a periodic stimulus[3,19,27]. This interplay between excitation and inhibition at the level of the cortex provides a "window of opportunity" for generating suprathreshold cortical responses[19] that match the dynamic range of the stimulus. During repetitive stimulation, feed-forward inhibition onto cortical excitatory cells decreases, owing to depression of both thalamocortical and corticocortical synapses, leading to an increase in the integration window of excitatory responses[19]. Given that the effects of adaptation are strongly dependent upon the nature of the adapting stimulus[18,22], it remains to be seen how adapting inputs of varying strength and statistical structure would shape the cortical sensitivity. Taken together, our results here suggest a dynamically evolving relationship between thalamic timing precision and its impact on cortex that could be a key element in the observed perceptual effects of adaptation.

Neuronal synchrony is thought to be important in sensory function and cognition[28], and such precise timing has been implicated in neural coding[26,29]. Thalamic synchrony has been previously proposed as an important component in generating cortical response properties in the vibrissal pathway[17,30]. In response to a single sensory stimulus, the temporal precision of thalamic input influences the cortical response to a greater extent than the overall thalamic firing rate[17], and high-velocity vibrissal stimuli induce synchronous thalamic firing within a barreloid[18,24]. Here, we show that although the cortical response is indeed sensitive to stimulus intensity in the nonadapted state[17], stimulus intensity can modulate thalamic synchrony more effectively in the adapted than nonadapted state. This results in better discrimination performance based on downstream neural firing activity due to enhanced sensitivity in the adapted state. Although the precise timing of thalamic firing is thought to be primarily generated by the strong inputs from trigeminal brainstem afferents, the adaptation of inhibitory input from thalamic reticular nucleus also likely modulates VPm synchrony[31].

It has recently been shown that weak pairwise correlations across neurons can have important implications for the large-scale network[25]. However, the effect of pairwise correlations on coding strategies is still very much in debate[32,33], and the implications in the context of adaptation are unclear. The measurements we provide here are comparative in nature. That is, we characterize the shift in pairwise correlations from nonadapted to adapted states. We implicitly assume that the relationship between the weak pairwise correlations and the coding strategies of the large-scale network would be preserved through adaptation, but this remains an open question.

Rats and other rodents rely extensively on their tactile sense to navigate and perceive the external world. It has been shown that this sensory modality is endowed with the capability for fine texture discrimination[34,35]. When in contact with a textured surface, the vibrissae resonate transiently during discrete, high-velocity 'slip-stick' events[36–38]. The rate and pattern of these high-velocity vibrissa transients varies with the properties of the texture and with the self motion, resulting in patterns of temporally precise, stimulus-locked spiking activity, described as a "kinetic signature" of the textured surface[35]. Thus, the discrimination between different textures potentially involves the discrimination between patterns of velocity transients, on the basis of corresponding patterns of cortical activation. In the natural environment, rats use foveal whisking to identify and palpate objects of interest[39], generating high-frequency vibrations of the vibrissae (hundreds to thousands of hertz) for hundreds of milliseconds[35]. Such persistent activation of the pathway may put the brain in an adapted state, resulting in an enhanced discriminability of the relevant features of the texture, as has been previously proposed[40]. In addition to surface texture properties, the vibrissal system also provides information to the animal that is useful for object localization[41], aperture discrimination[42], and stimulus detection[21] and discrimination[43], in many cases involving the inference of a single transient contact, such as that presented in the detection task in this study. Given this dichotomy, it has been proposed that the lemniscal and paralemniscal pathways separately process vibrissa motion in parallel for texture coding and object contact, respectively[1]. The thalamic data shown here were identified as VPm in origin, and thus part of the lemniscal tract, on the basis of stereotaxic coordinates and response latencies (**Supplementary Note 5**). Although it is not presently known whether the seemingly disparate types of sensory information involved in discrimination and contact detection are mutually exclusive behaviorally, nor is it known to what extent the pathways interact as the self motion of the animal shapes the sensory input in a continuous manner[44], our study does demonstrate that the lemniscal pathway preserves sufficient information for dynamically switching between different coding strategies in behavioral contexts.

The properties of the sensory input serve to control overall activation and timing precision across neurons in the local populations[29], suggesting a potential role for thalamic synchrony in controlling information flow to cortex in the dynamic, natural sensory environment[29]. However, the thalamocortical network is also strongly influenced by CNS inputs that are associated with states of arousal. Specifically, activation of the reticular formation influences thalamus and cortex both directly and indirectly. Recently, it was shown that electrical stimulation of the basal forebrain serves to enhance discriminability across the thalamocortical circuit[45], presumably through modulations in thalamic synchrony. Neurotransmitters associated with arousal act to depolarize the thalamus, shifting the firing properties[46] and increasing the spontaneous firing rates of thalamocortical neurons[47]. Increased thalamic activity associated with arousal leads to an 'adapted' state in cortex characterized by low background firing, higher signal-to-noise ratio and sharpened receptive fields[47]. Given the differences in thalamocortical activity between the anesthetized and awake animal[46,47], it remains an open question as to how the neural phenomenon described here is affected by wakefulness and higher level, top-down attentional processes. Nevertheless, adaptation to a periodic tactile input has been shown to enhance spatial localization and frequency discrimination in humans[8–10].

Although the issue of rate versus temporal coding has been vigorously debated in the literature, there is now fairly widespread agreement that the various pathways in the brain likely operate on a range of time scales[48], and that the relevant time scales likely change with time and context. The time scale of firing activity across upstream neural populations is transferred to downstream neural activity by the dynamics of synaptic integration across the brain regions, and thus the range of time scales of synaptic integration ultimately determines the relevant time scales of the neural code. The results here suggest that with respect to stimulus strength (angular velocity), the thalamic population operates with a temporal code that is transformed to a rate code across the thalamocortical synapse. Moreover, the dynamics of thalamocortical integration change in a complex way

with adaptation[19], which, along with modulation of synchronization across the thalamic population, leads to a dynamic gating of information flow to cortex, consistent with the hypothesis that adaptation in the rat vibrissa system could serve to switch from a mode that facilitates detection to one that facilitates discrimination. Studies pairing electrophysiological recordings with behavior that permit the direct comparison of neurometric and psychometric performance suggest a complex relationship between the time course of cortical activity and perception[49]. Although it is not likely that cortical layer 4, or even primary somatosensory cortex as a whole, is solely responsible for generating perceptions, the emergence of feature selectivity across the thalamocortical synapse forms the constituent elements upon which perception is ultimately built.

## METHODS

Methods and any associated references are available in the online version of the paper at http://www.nature.com/natureneuroscience/.

*Note: Supplementary information is available on the Nature Neuroscience website.*


### ACKNOWLEDGMENTS

We would like to thank Jose-Manuel Alonso for comments at various points of this work and Daniel Millard for assistance in calibration and testing of the piezoelectric stimulator. This work was supported by the US National Institutes of Health (R01NS48285).


### AUTHOR CONTRIBUTIONS

Q.W. and G.B.S. conceived the study. Q.W., R.M.W. and G.B.S. designed the experiments. Q.W. performed the experiments. Q.W. and G.B.S. analyzed the data, and Q.W., R.M.W. and G.B.S. wrote the paper.

### COMPETING FINANCIAL INTERESTS

The authors declare no competing financial interests.

Published online at http://www.nature.com/natureneuroscience/.
Reprints and permissions information is available online at http://npg.nature.com/reprintsandpermissions/.




1. Ahissar, E., Sosnik, R. & Haidarliu, S. Transformation from temporal to rate coding in a somatosensory thalamocortical pathway. *Nature* **406**, 302–306 (2000).
2. Chung, S., Li, X. & Nelson, S.B. Short-term depression at thalamocortical synapses contributes to rapid adaptation of cortical sensory responses in vivo. *Neuron* **34**, 437–446 (2002).
3. Higley, M.J. & Contreras, D. Balanced excitation and inhibition determine spike timing during frequency adaptation. *J. Neurosci.* **26**, 448–457 (2006).
4. Khatri, V., Hartings, J.A. & Simons, D.J. Adaptation in thalamic barreloid and cortical barrel neurons to periodic whisker deflections varying in frequency and velocity. *J. Neurophysiol.* **92**, 3244–3254 (2004).
5. Maravall, M., Petersen, R.S., Fairhall, A.L., Arabzadeh, E. & Diamond, M.E. Shifts in coding properties and maintenance of information transmission during adaptation in barrel cortex. *PLoS Biol.* **5**, e19 (2007).
6. Fairhall, A.L., Lewen, G.D., Bialek, W. & de Ruyter van Steveninck, R.R. Efficiency and ambiguity in an adaptive neural code. *Nature* **412**, 787–792 (2001).
7. Barlow, H. Possible principles underlying the transformation of sensory messages. in *Sensory Communication* (ed. Rosenblith, W.A.) 217–234 (MIT Press, 1961).
8. Goble, A.K. & Hollins, M. Vibrotactile adaptation enhances frequency discrimination. *J. Acoust. Soc. Am.* **96**, 771–780 (1994).
9. Goble, A.K. & Hollins, M. Vibrotactile adaptation enhances amplitude discrimination. *J. Acoust. Soc. Am.* **93**, 418–424 (1993).
10. Tannan, V., Simons, S., Dennis, R.G. & Tommerdahl, M. Effects of adaptation on the capacity to differentiate simultaneously delivered dual-site vibrotactile stimuli. *Brain Res.* **1186**, 164–170 (2007).
11. Crick, F. Function of the thalamic reticular complex: the searchlight hypothesis. *Proc. Natl. Acad. Sci. USA* **81**, 4586–4590 (1984).
12. Steriade, M., McCormick, D.A. & Sejnowski, T.J. Thalamocortical oscillations in the sleeping and aroused brain. *Science* **262**, 679–685 (1993).
13. Lesica, N.A. & Stanley, G.B. Encoding of natural scene movies by tonic and burst spikes in the lateral geniculate nucleus. *J. Neurosci.* **24**, 10731–10740 (2004).
14. Swadlow, H.A. & Gusev, A.G. The impact of 'bursting' thalamic impulses at a neocortical synapse. *Nat. Neurosci.* **4**, 402–408 (2001).
15. Usrey, W.M., Alonso, J.-M. & Reid, R.C. Synaptic interactions between thalamic inputs to simple cells in cat visual cortex. *J. Neurosci.* **20**, 5461–5467 (2000).
16. Roy, S.A. & Alloway, K.D. Coincidence detection or temporal integration? What the neurons in somatosensory cortex are doing. *J. Neurosci.* **21**, 2462–2473 (2001).
17. Pinto, D.J., Brumberg, J.C. & Simons, D.J. Circuit dynamics and coding strategies in rodent somatosensory cortex. *J. Neurophysiol.* **83**, 1158–1166 (2000).
18. Temereanca, S., Brown, E.N. & Simons, D.J. Rapid changes in thalamic firing synchrony during repetitive whisker stimulation. *J. Neurosci.* **28**, 11153–11164 (2008).
19. Gabernet, L., Jadhav, S.P., Feldman, D.E., Carandini, M. & Scanziani, M. Somatosensory integration controlled by dynamic thalamocortical feed-forward inhibition. *Neuron* **48**, 315–327 (2005).
20. Britten, K.H., Shadlen, M.N., Newsome, W.T. & Movshon, J.A. The analysis of visual motion: a comparison of neuronal and psychophysical performance. *J. Neurosci.* **12**, 4745–4765 (1992).
21. Stüttgen, M.C. & Schwarz, C. Psychophysical and neurometric detection performance under stimulus uncertainty. *Nat. Neurosci.* **11**, 1091–1099 (2008).
22. Ganmor, E., Katz, Y. & Lampl, I. Intensity-dependent adaptation of cortical and thalamic neurons is controlled by brainstem circuits of the sensory pathway. *Neuron* **66**, 273–286 (2010).
23. Bruno, R.M. & Simons, D.J. Feedforward mechanisms of excitatory and inhibitory cortical receptive fields. *J. Neurosci.* **22**, 10966–10975 (2002).
24. Bruno, R.M. & Sakmann, B. Cortex is driven by weak but synchronously active thalamocortical synapses. *Science* **312**, 1622–1627 (2006).
25. Schneidman, E., Berry, M.J., Segev, R. & Bialek, W. Weak pairwise correlations imply strongly correlated network states in a neural population. *Nature* **440**, 1007–1012 (2006).
26. Wang, H.-P., Spencer, D., Fellous, J.-M. & Sejnowski, T.J. Synchrony of thalamocortical inputs maximizes cortical reliability. *Science* **328**, 106–109 (2010).
27. Heiss, J.E., Katz, Y., Ganmor, E. & Lampl, I. Shift in the balance between excitation and inhibition during sensory adaptation of S1 neurons. *J. Neurosci.* **28**, 13320–13330 (2008).
28. Womelsdorf, T., Fries, P., Mitra, P.P. & Desimone, R. Gamma-band synchronization in visual cortex predicts speed of change detection. *Nature* **439**, 733–736 (2006).
29. Butts, D.A. *et al.* Temporal precision in the neural code and the timescales of natural vision. *Nature* **449**, 92–95 (2007).
30. Khatri, V., Bruno, R.M. & Simons, D.J. Stimulus-specific and stimulus-nonspecific firing synchrony and its modulation by sensory adaptation in the whisker-to-barrel pathway. *J. Neurophysiol.* **101**, 2328–2338 (2009).
31. Hartings, J.A., Temereanca, S. & Simons, D.J. Processing of periodic whisker deflections by neurons in the ventroposterior medial and thalamic reticular nuclei. *J. Neurophysiol.* **90**, 3087–3094 (2003).
32. Romo, R., Hernández, A., Zainos, A. & Salinas, E. Correlated neuronal discharges that increase coding efficiency during perceptual discrimination. *Neuron* **38**, 649–657 (2003).
33. Zohary, E., Shadlen, M.N. & Newsome, W.T. Correlated neuronal discharge rate and its implications for psychophysical performance. *Nature* **370**, 140–143 (1994).
34. Carvell, G.E. & Simons, D.J. Biometric analyses of vibrissal tactile discrimination in the rat. *J. Neurosci.* **10**, 2638–2648 (1990).
35. von Heimendahl, M., Itskov, P.M., Arabzadeh, E. & Diamond, M.E. Neuronal activity in rat barrel cortex underlying texture discrimination. *PLoS Biol.* **5**, e305 (2007).
36. Ritt, J.T., Andermann, M.L. & Moore, C.I. Embodied information processing: vibrissa mechanics and texture features shape micromotions in actively sensing rats. *Neuron* **57**, 599–613 (2008).
37. Wolfe, J. *et al.* Texture coding in the rat whisker system: slip-stick versus differential resonance. *PLoS Biol.* **6**, e215 (2008).
38. Jadhav, S.P., Wolfe, J. & Feldman, D.E. Sparse temporal coding of elementary tactile features during active whisker sensation. *Nat. Neurosci.* **12**, 792–800 (2009).
39. Berg, R.W. & Kleinfeld, D. Rhythmic whisking by rat: retraction as well as protraction of the vibrissae is under active muscular control. *J. Neurophysiol.* **89**, 104–117 (2003).
40. Moore, C.I., Nelson, S.B. & Sur, M. Dynamics of neuronal processing in rat somatosensory cortex. *Trends Neurosci.* **22**, 513–520 (1999).
41. Mehta, S.B., Whitmer, D., Figueroa, R., Williams, B.A. & Kleinfeld, D. Active spatial perception in the vibrissa scanning sensorimotor system. *PLoS Biol.* **5**, e15 (2007).
42. Krupa, D.J., Matell, M.S., Brisben, A.J., Oliveira, L.M. & Nicolelis, M.A.L. Behavioral properties of the trigeminal somatosensory system in rats performing whisker-dependent tactile discriminations. *J. Neurosci.* **21**, 5752–5763 (2001).
43. Gerdjikov, T.V., Bergner, C.G., Stüttgen, M.C., Waiblinger, C. & Schwarz, C. Discrimination of vibrotactile stimuli in the rat whisker system: behavior and neurometrics. *Neuron* **65**, 530–540 (2010).
44. Jenks, R.A., Vaziri, A., Boloori, A.-R. & Stanley, G.B. Self-motion and the shaping of sensory signals. *J. Neurophysiol.* **103**, 2195–2207 (2010).
45. Goard, M. & Dan, Y. Basal forebrain activation enhances cortical coding of natural scenes. *Nat. Neurosci.* **12**, 1444–1449 (2009).
46. Stoelzel, C.R., Bereshpolova, Y. & Swadlow, H.A. Stability of thalamocortical synaptic transmission across awake brain states. *J. Neurosci.* **29**, 6851–6859 (2009).
47. Castro-Alamancos, M.A. Role of thalamocortical sensory suppression during arousal: focusing sensory inputs in neocortex. *J. Neurosci.* **22**, 9651–9655 (2002).
48. König, P., Engel, A.K. & Singer, W. Integrator or coincidence detector? The role of the cortical neuron revisited. *Trends Neurosci.* **19**, 130–137 (1996).
49. Luna, R., Hernandez, A., Brody, C.D. & Romo, R. Neural codes for perceptual discrimination in primary somatosensory cortex. *Nat. Neurosci.* **8**, 1210–1219 (2005).

## ONLINE METHODS

**Surgery and preparation.** Forty female adult Sprague Dawley rats (220–330 g) were used in the study. All procedures were approved by the Institutional Animal Care and Use Committees at Harvard University and Georgia Institute of Technology. Briefly, rats were sedated with 2% vaporized isoflurane and anesthetized with sodium pentobarbital (50 mg per kilogram body weight, intraperitoneally, initial dose); supplementary doses were given as needed to maintain a surgical level of anesthesia, confirmed by measurements of heart rate, respiration, and eyelid and pedal reflexes to aversive stimuli (toe or tail pinch). Body temperature was maintained at 37 °C by a servo-controlled heating blanket (FHC). The animal was mounted on a stereotaxic device (Kopf Instruments) on a floating table in preparation for the surgery and subsequent recordings. Atropine (0.5 mg $kg^{-1}$, subcutaneously) was injected, and 2% (wt/vol) lidocaine solution was applied to the tissue on top of the head. A small craniotomy was made on the left hemisphere over the barrel cortex (stereotaxic coordinates: 1.0–4.0 mm caudal to the bregma, and 4.0–7.0 mm lateral to the midline) and over the ventral posteromedial nucleus (VPm) of the thalamus (2.0–4.0 mm caudal, 2.5–3.5 mm lateral to the midline)[4]. The dura mater was then carefully removed. After the recording session, the animal was killed with an overdose of sodium pentobarbital.

**Electrophysiological recordings.** Single-unit extracellular recordings were obtained by using either tungsten microelectrodes (~5–8 MΩ, FHC) or quartz-insulated platinum/tungsten (90%/10%) microelectrodes (~2–6 MΩ, Thomas Recording). First, a microelectrode was advanced into VPm. After the principal whisker of the well-isolated VPm cell was identified, a microelectrode was positioned perpendicular to the pial surface and advanced into the homologous barrel according to the barrel map, until a single unit was located that was homologous to the VPm barreloid and had a fairly restricted whisker input. For each thalamic cell, a shift in latency with adaptation greater than 20 ms resulted in exclusion of the cell from the study to ensure that the thalamic sample consisted solely of neurons from VPm, rather than posteromedial complex[1]. A total of 32 thalamocortical pairs were recorded over the entire duration (>1 h) of the stimulus protocol (30 cortical neurons; 32 VPm neurons, two of which were recorded simultaneously with another VPm neuron).

A total of 19 simultaneously recorded pairs of VPm neurons were recorded using a 20-channel microdrive system (Mini-Matrix, Thomas Recording). Three to five pulled and beveled quartz-insulated platinum/tungsten (90%/10%) microelectrodes (4–6 MΩ, 80 μm in diameter) were guided through a five-channel linear microdrive head (Head05-lin-305-305-b, Thomas Recording) with 305 μm interelectrode spacing, then positioned approximately 100 μm apart on the cortical surface through a custom-made glass guide tube (tip diameter, approximately 250 μm). Subsequently, these electrodes were slowly advanced into the brain independently at 1 μm resolution. All 19 pairs presented here were recorded when the two electrodes were in the same barreloid.

Data were collected using a 32-channel data acquisition system (Plexon). Neuronal signals were amplified, band-pass filtered (500 Hz–5 kHz), and digitized at 40 kHz per channel. Recordings were analyzed using the OfflineSorter software suite (Plexon) to assign the recorded spike waveforms to single units on the basis of standard template matching techniques and physiologically plausible refractory periods. All cortical cells were located at stereotaxic depths of 500–900 μm, presumably within cortical layer IV. Cortical cells were classified as RSUs (putative excitatory neurons) or fast spiking units (putative inhibitory interneurons) on the basis of the width of action potential waveform. A recorded neuron was classified as an RSU when the initial trough was > 200 μs and the total duration of the waveform was > 850 μs (see **Supplementary Fig. 1**), and the spontaneous firing rate <1 Hz (ref. 23). Following this online classification, only RSUs were recorded in the subsequent stimulus presentation.

**Whisker stimulation.** Whiskers were trimmed at ~12 mm from the face and inserted into a 30-mm glass pipette fixed to the end of a calibrated multilayered piezoelectric bimorph bending actuator (range of motion, 1 mm; bandwidth, 300 Hz; Polytec PI) positioned 10 mm from the vibrissal pad. Rostral–caudal pulse deflections consisted of exponential rising and falling phases (99% rise time, 5 ms; 99% fall time, 5 ms). Pulses with amplitude of 680 μm (800 deg $s^{-1}$) were used as adapting stimuli (15 deflections at 12 Hz). The probe stimulus was presented as the 16th deflection of the 12-Hz stimulus, and thus there was an 83 ms delay between the last deflection of the adapting stimulus and the probe. Pulses with angular deflection velocities of 50, 100, 300, 600 and 1,200 deg $s^{-1}$ were used as probe stimuli (s1–s5, respectively), where angular velocity was quantified as the average rate of rise to maximum amplitude. The pulses had a fixed duration (10 ms), and thus the peak amplitude co-varied with the velocity[22]. Isolated deflections (probe stimuli) were presented in the presence or absence of the adapting stimulus, forming stimulus blocks that were presented in an interleaved fashion. The interval between stimulus blocks was 5 s for probe stimuli preceded by adapting stimuli (that is, 15 adapting deflections plus one probe deflection) and 1.5 s for probe stimuli. Stimulus blocks with different angular velocities of the probe stimulus were randomized. Each stimulus block was presented 100–120 times.

**Response analysis.** Mean spike count and variance were calculated from the trial-to-trial spike count in the 30 ms poststimulus window following each deflection. As further confirmation of recording sites, response latencies for cortical and thalamic units were quantified in both the nonadapted and adapted states: cortical (nonadapted, 7.6 ± 0.23 ms; adapted, 13.3 ± 0.91 ms), VPm (nonadapted, 4.8 ± 0.15 ms; adapted, 10.9 ± 0.88 ms, mean ± s.e.m.), consistent with cortical layer 4 RSUs and VPm neurons, respectively. Mean population spike count was defined as the mean spike count times the number of assumed neurons with identical statistics. Adaptation ratio was calculated by dividing the average spike count elicited by the last three pulses by the average spike count elicited by the first three pulses. The spike count distributions were fit to gamma distributions (see **Supplementary Note 1**).

**Ideal observer: detection.** We first quantified the effects of adaptation on our ability to detect the presence of vibrissa deflection in the presence of noise. The noise distribution was evaluated by measuring the spontaneous spike count within a random 30-ms window within a 1-s period following the probe stimulus for the adapted state, and within a 1-s period preceding the probe stimulus for the nonadapted state. We used the parameterized distributions of the spike count for stimulus-evoked activity and for non–stimulus evoked spontaneous activity (see **Supplementary Fig. 3a**), and applied classical signal detection theory[20,21]. The ROC curve expresses the probability of a false alarm (incorrectly attributing the activity to signal when it was actually noise) versus the probability of a hit (correctly attributing the activity to signal when it was actually signal). To summarize the performance, the AUROC was calculated for both nonadapted and adapted states.

**Ideal observer: discrimination.** The ideal observer was used to discriminate between five different possible stimuli (s1, s2 … s5) on the basis of the observed activity. The spike count distribution associated with each stimulus intensity was parameterized with a gamma distribution, with the performance of the observer determined by the amount of overlap between the different distributions. We considered the ideal observer to be a Bayesian decoder using maximum likelihood estimation to assign an observed response to a particular stimulus intensity. The likelihood function for a particular stimulus $s_i$ is denoted $p(r \mid s_i)$, where $r$ is the observed spike count. Therefore, $p(s_i \mid r) = p(\mathrm{r} \mid \mathrm{s_i}) \times p(s_i)/p(r)$. For the case in which the stimuli are presented with equal probability, the ideal observer assigns the observation to the distribution for which the likelihood function is maximal. The performance matrix is a 5 × 5 matrix in which the $(i,j)$ element is the probability of assigning the observed response to stimulus $s_j$ when the real stimulus is $s_i$. The overall performance of the decoder is the sum of all diagonal elements of the performance matrix.

After we parameterized the gamma distributions of neural activity, the theoretical performance of the ideal observer using the Bayesian decoding strategy was determined. The probability that the Bayesian decoder will choose $s_i$ when the stimulus presented is actually $s_j$ is the area of the region of $p(r \mid s_j)$ in which the $p(r \mid s_i)$ is maximal (**Supplementary Fig. 4**). Percentage change in discrimination performance was calculated as the change in performance from the nonadapted to adapted states, divided by the performance in the adapted state. Note that adaptation has also been shown to sharpen directional tuning[50]. Here, discrimination was also performed for cortical response to direction of whisker deflection (**Supplementary Note 3**).

**Simulation.** A leaky integrate-and-fire model was used in all simulations. The model neuron had a resting potential of $V_{rest} = -70$ mV and membrane time constant of 5 ms. When the membrane potential reached −55 mV, the model neuron fired an action potential and was reset to −65 mV. Upon arrival of a presynaptic




doi:10.1038/nn.2670

spike, an EPSC (0.4 nA, exponentially decaying with a time constant of 0.25 ms) was injected into the model neuron, whose membrane had a conductance of 2.86 nS (350 MΩ). White synaptic noise (maximum amplitude, 0.04 nA) was added to adjust the variance in trial-to-trial spike count while maintaining the same mean spike count, tuned to match our experimental observations. The integration window of the model neuron was normally distributed across trials, with a mean ± s.d. of 12 ± 2 ms in the nonadapted state, and 22 ± 2 ms in the adapted state[19]. Thalamic spikes that arrived later than the integration window were discarded. To generate the thalamic input to the integrate-and-fire model of **Fig. 7b**, all thalamic spikes across all experimentally recorded neurons in response to a specific stimulus were pooled. For each simulated trial, ten thalamic responses were randomly selected from the pool and used as input to the model. This was repeated for 3,200 trials, to generate an amount of simulated data comparable to the amount of experimental data (across all cells and trials). Note that recent studies have suggested that the number of thalamic inputs to recipient cortical layer 4 neurons may be more on the order of 100 (ref. 24). Because we constructed the VPm population from randomly selected trials of the recorded VPm inputs, we were limited by the number of recorded trials. However, when the analysis was repeated for 20 and 30 trials, there was no significant change in the results, suggesting that our smaller sample captures the essential relationship. All simulations were repeated with a quadratic (squaring) nonlinearity in the output of the integrate-and-fire model, resulting in no qualitative difference. Further, simulations were repeated while including a simple model of synaptic depression[2]. Specifically, during the adapted state, we attenuated the EPSC caused by the thalamic spike by 40%. This resulted in qualitatively very similar results to those shown here.

**Cross-correlation analysis.** A subset of thalamocortical pairs was identified as likely to be monosynaptically connected through cross-correlation analysis. Given the low spontaneous firing rates of neurons in primary somatosensory cortex, each pair was weakly driven with a 700-μm amplitude, 4-Hz sinusoidal deflection of the principal whisker[23,24]. A thalamocortical pair was identified as monosynaptically connected based on a sharp peak in the cross-correlogram at a very short (~2 ms) latency[14,23]. Due to the high degree of connectivity between neurons in a VPm barreloid and neurons in the corresponding layer 4 barrel[24], it is likely that more of the pairs were monosynaptically connected than those conservatively reported here. Cross-correlation analysis was also used for stimulus-evoked activity to assess the synchrony across thalamocortical pairs and the effects of adaptation on this relationship. The cross-correlogram was constructed in the same manner as above, and the synchrony was defined as the central area under the cross-correlogram within a synchrony window as in ref. 18. The shuffled cross-correlogram was also generated for comparison[23] (**Supplementary Figs. 9** and **10**).

**Statistical analysis.** Shapiro-Wilk normality test was used to assess the normality of data before performing statistical tests. If the samples were normally distributed, Student's *t*-test was used. Otherwise, the Mann-Whitney *U*-test was used for unpaired samples and the Wilcoxon signed-rank test was used for paired samples.

50. Khatri, V. & Simons, D.J. Angularly nonspecific response suppression in rat barrel cortex. *Cereb. Cortex* **17**, 599–609 (2007).